Science of the Total Environment 636 (2018) 1279–1290

Contents lists available at ScienceDirect

Science of the Total Environment

journal homepage: www.elsevier.com/locate/scitotenv

Single particle characterization of summertime particles in Xi'an (China)

Yang Chen [a,b], Huanwu Liu [c], Fumo Yang [d,a,e,*], Shumin Zhang [f], Wentao Li [c], Guangming Shi [d,a], Huanbo Wang [a], Mi Tian [a], Suixin Liu [b], Rujin Huang [b], Qiyuan Wang [b], Ping Wang [b], Junji Cao [b,g,**]

[a] Chongqing Institute of Green and Intelligent Technology, Chinese Academy of Sciences, Chongqing 400714, China
[b] Key Lab of Aerosol Chemistry & Physics, Institute of Earth Environment, Chinese Academy of Sciences, Xi'an 710061, China
[c] Xi'an Environmental Monitor Station, Xi'an 710061, China
[d] College of Architecture and Environment, Sichuan University, Chengdu 610065, China
[e] Center for Excellence in Urban Atmospheric Environment, Institute of Urban Environment, Chinese Academy of Sciences, Xiamen 361021, China
[f] School of Basic Medical Sciences, North Sichuan Medical College, Nanchong 637000, Sichuan, China
[g] Institute of Global Environmental Change, Xi'an Jiaotong University, Xi'an 710049, China

HIGHLIGHTS

- Traffic-related particles were up to 83% in the SPAMS dataset.
- Local aging and short-distance transport were the major PM originations.
- Urban particles were more acidic with aerodynamic diameter < 0.8 μm.
- SOA formed on OC-related particles due to mass transfer or diffusion limitations.
- The enrichment of oxalate was observed in Fe-Nit particles.

GRAPHICAL ABSTRACT

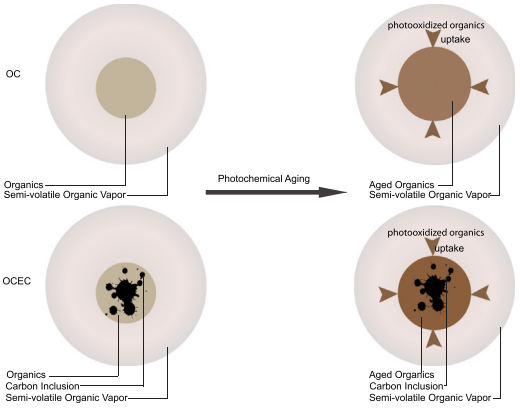

ARTICLE INFO

Article history:
Received 14 March 2018
Received in revised form 28 April 2018
Accepted 28 April 2018
Available online 9 May 2018

Editor: Jianmin Chen

Keywords:
SPAMS
Mixing state
Aerosol acidity
Source
Origination

ABSTRACT

Urban particles in Xi'an during summertime were investigated using a single particle aerosol mass spectrometer (SPAMS). Twelve major particle types were resolved, including EC-Sul-Nit (-Sul stands for sulfate, -Nit for nitrate, and 25% in number fraction), EC(6%), EC-Nit (12%) and, EC-Sul (8%), mixed Elemental and Organic Carbon-Sul-Nit (9%), ECOC-Sul (8%), K-Nit (12%), OC (8%), NaK-Nit (5%), Fe-Nit (5%), Ca-Nit (1%), and Other (1%). Among these particle types, chemical composition, mixing state, and wind-dependent analyses were conducted to investigate their originations and sources. During summertime, traffic-related particles were up to 83% in the SPAMS dataset. Two major originations of urban particles were identified, including the local aging and short-distance transport mainly from the southeast. Size-resolved relative acidity ((sulfate + nitrate) / ammonium) analysis suggested that urban particles were more acidic with an aerodynamic diameter < 0.8 μm. In diurnal cycle, the strongest relative aerosol acidity occurred between 7:00 and 9:00 in the morning when relative humidity was between 60 and 70%, and the weakest acidity occurred from 13:00–15:00. Among all major particle types, OC and K-Nit had stronger relative aerosol acidity than other types. Mixing state analysis indicated that the organic semi-volatile vapor is favorable to

* Correspondence to: F. Yang, College of Architecture and Environment, Sichuan University, Chengdu 610065, China.
** Correspondence to: J. Cao, Key Lab of Aerosol Chemistry & Physics, Institute of Earth Environment, Chinese Academy of Sciences, Xi'an 710061, China.
E-mail addresses: fmyang@cigit.ac.cn (F. Yang), cao@loess.llqg.ac.cn (J. Cao).

https://doi.org/10.1016/j.scitotenv.2018.04.388

condense on the OC-related particles (OC, ECOC-Sul, and ECOC-Sul-Nit) as evidence that primary organic aerosol (POA) would enhance the secondary organic aerosol (SOA) formation via gas-to-particle phase partitioning when SOA and POA are miscible. Oxalate also tends to be observed in the droplet of OC-related particles. In addition, the enrichment of oxalate was observed in Fe-Nit particles. This study would be useful to understand the characterization, mixing state, source, origination, and processing of urban particles during summertime in Xi'an as well as the urban areas in the Guanzhong Basin.

1. Introduction

Fine particulate matter ($PM_{2.5}$) has impacts on visibility, climate, and human health (Seinfeld and Pandis, 2016). $PM_{2.5}$ is a major pollutant in urban areas of China (Tao et al., 2017). The first large-scale particulate pollution occurred in January 2013, and approximately 800 million people were influenced (Huang et al., 2014). In the following years, air-polluted areas in China, including Beijing-Tianjin-Hebei area, Yangtze River Delta, Peral River Delta, Guanzhong basin, and Sichuan basin have been drawing worldwide attention (Cao, 2014).

China has been making efforts on improving air quality in these areas. Understanding emission sources are essential for abating $PM_{2.5}$. Various PM emissions and complicated atmospheric processes lead to the demand of area-specific characterizations of particulate pollution. For example, in Beijing-Tianjin-Hebei area, coal burning, and industry have been identified as the primary sources (Chen et al., 2014; Ma et al., 2016; Sun et al., 2013). In Yangtze River Delta, other than local emissions from industry and traffic, pollutants from Northern China via transport are responsible for poor air quality (Cao et al., 2012; Huang et al., 2013; Zhang et al., 2014; Zhang et al., 2009). In Sichuan basin, anthropogenic biomass burning activities have been identified as one of the most important sources (Chen et al., 2017).

Among the polluted areas, Guanzhong basin is located in Northwestern China, at the southern edge of Loess Plateau, surrounded by Qinling-Dabashan mountains in the south. In the basin, the plain is ~36,000 km^2 and with a population of 24.0 million (Sun et al., 2017). The basin has been suffering poor air quality in recent years (Chen et al., 2016; Li et al., 2016; Shen et al., 2011). Air quality in the basin is influenced by fugitive dust (Cao et al., 2008; Li et al., 2016), biomass burning (Sun et al., 2017), traffic, coal burning (Chen et al., 2016), and secondary aerosol (Huang et al., 2014; Wang et al., 2017). In winter, coal and biomass burning for heating purpose caused severe air pollution (Chen et al., 2016; Wang et al., 2017). Meanwhile, unfavorable meteorological conditions, such as temperature inversion and low-level horizontal wind speed, also contribute to extreme haze episodes (Bei et al., 2016). Furthermore, low-level horizontal wind speed is common in the basin, annually 200 days per year (Huang et al., 2017). Therefore, air pollutants in the basin are difficult to disperse. Additionally, Bei et al. (2016) proposed that emissions in the basin need to be mitigated by >90% to meet the excellent level of the Chinese National Air Quality Standard for $PM_{2.5}$ under these extremely unfavorable meteorological conditions.

Xi'an is the most important megacity in the Guanzhong Basin, studies of PM characterization, source, and trends have been conducted for years (Cao, 2014). A study of chemical composition and mixing state of urban PM during the winter haze period has been reported (Chen et al., 2016). However, during summertime, such kind of characterization has not been performed. The aims of this study are (1) to characterize chemical composition and mixing state of urban particles in a megacity of Xi'an during summertime, (2) to investigate source and origination of urban PM, and (3) to study the atmospheric processing of particles including aerosol acidity evolution and the secondary formation.

2. Methods

2.1. Field measurements

Fig. 1 shows the map of Xi'an city and major roads (at least 4-lane dual carriageway). The sampling site (108.949° E, 34.350° N) is on the ground level, in the center of Xi'an Urban Sports Park. The site is surrounded by residential communities, 9 km away from the city center. There are no significant industrial facilities with a distance of 10 km. $PM_{2.5}$ was monitored using a tapered element oscillating microbalance (TEOM 1405, Thermo Scientific). Trace gases such as NO, NO_2, O_3, SO_2, and CO were also monitored using Thermo 42*i*, 49*i*, 43*i*, 48*i*, respectively.

A single particle aerosol mass spectrometer (SPAMS 0525, Hexin, China) was deployed on the site to collect data of size-resolved chemical composition and mixing state of urban particles from 08/08/2015 to 08/21/2015. A diffusive dryer was installed in front of the sampling inlet to avoid the influence of varying RH. A technical description of SPAMS is available in literature (Li et al., 2011). In principle, particles are sampled into SPAMS using an aerodynamic lens which transmits particles in size range 0.1–2.0 μm efficiently to form a particle beam before their sizes are determined. The vacuum aerodynamic diameter (D_{va}) of each particle is calculated by the time-of-flight when crossing two pre-positioned laser beams (Nd: YAG, 532 nm) inside the sizer unit. Particles subsequently enter the mass spectrometer unit and are ionized using an Nd: YAG laser operating at a wavelength of 266 nm. The yielding bipolar ions are analyzed in a time-of-flight mass spectrometer.

2.2. SPAMS data analysis

The SPAMS particle lists were imported into the YAADA toolkit (run in Matlab 2012b) for analysis. An adaptive resonance theory based neural network algorithm (ART-2a) was applied to cluster the particles with a vigilance factor of 0.70, a learning rate of 0.05, and 20 iterations (Song et al., 1999). This procedure produced 157 particle clusters, many of which exhibited identical mass spectra with slight differences in ion peak areas. A well-established combining strategy based on similar temporal trend, mass spectra, and size distribution was adopted to merge these 157 particle types into 12 distinct groups (Dall'osto and Harrison, 2006).

All the particle clusters were labeled with a scheme that has been regularly used in literature (Healy et al., 2010; Pratt and Prather, 2012). The scheme focuses on the dominant species starting from the positive mass spectrum, with an order of ions sorted by their relative intensities. The common species include elemental carbon (C^+ and C^-), organic species ($C_xH_y^+$, $C_xH_yO_z^+$, CN^-, and CNO^-), ammonium (NH_4^+), potassium (K^+), sodium (Na^+), sulfate (HSO_4^-), phosphate (PO_3^-), and nitrate (NO_2^- and NO_3^-). For example, EC-Sulfate suggests that it is composed of internally mixed elemental carbon ions followed by sulfate. Since the strong signal of K^+ is common in mass spectra, the heading of K is only used when K^+ is the only dominant ion (*m*/*z* 39 and 41) in the positive mass spectrum. To keep names particle type short through the text, "-Nit" stands for nitrate, and "-Sul" for sulfate.

Fig. 1. Map of the sampling site, yellow lines indicate the major roads. The label G312 indicates the National Highway No. 312, and so forth.

3. Results and discussion

3.1. Size-resolved particle clusters characterization

A number of 475,951 ambient particles were collected with validated mass spectra (30 units above the baseline in peak area) from 08/08/2015 to 08/21/2015 with an overall hit rate (the number of hit particles over that of detected particles) of 23%. Twelve ART-2a clusters have been identified and assigned following the scheme mentioned in Section 2.2, including EC-Sul-Nit (-Sul stands for sulfate, -Nit for nitrate, and 25% in number), EC(6%), EC-Nit (12%), EC-Sul (8%), mixed Elemental and Organic Carbon-Sul-Nit (9%), ECOC-Sul (8%), K-Nit (12%), OC (8%), NaK-Nit (5%), Fe-Nit (5%), Ca-Nit (1%), and Other (1%). Some of clusters have complicated mass spectra and need to be interpreted in detail. For example, ECOC-Sul is pronounced in K^+, carbon ions, and OC fragments such as $[C_3H]^+$ (m/z 37), $[C_2HO]^+$ (m/z 41), $[CH_3CO]^+$ (m/z 43), $[C_4H_3]^+$ (m/z 51), $[C_5H_3]^+$ (m/z 63), and $[C_6H_2]^+$ (m/z 74). In the negative spectrum, $[CN]^-$ (m/z −26), $[Cl]^-$ (m/z −35 and −37), $[NO_2]^-$ (m/z −46), $[NO_3]^-$ (m/z −62), and sulfate (m/z −80 and −96) are present. ECOC-Sul-Nit is similar to ECOC-Sul (R^2 = 0.61) but aged with strong nitrate signals (Moffet and Prather, 2009; Pratt et al., 2011).

The ambient particle clusters can be further cataloged, including EC (EC, EC-Nit, EC-Sul, and EC-Sul-Nit, Fig. S1), OC-related (ECOC-Sul, ECOC-Sul-Nit, and OC, Fig. S2), dust-related (Ca-Nit and Fe-Nit), NaK-Nit, and K-Nit (Fig. S3). Overall, except the freshly-emitted EC particle type, strong uptake of nitrate was found in all particle types. The secondary nitrate formation was due to sufficient precursor (the average NO_x was 60 μg m^{-3}) and the strong solar radiation during summertime to produce HNO_3 (g) (Zhang et al., 2015). HNO_3 (g) can enter the particle phase via acid-base neutralization on the aerosol surface or dissolve in aerosol water (Seinfeld and Pandis, 2016). Notable that high temperature would lead to the decomposition of nitrate particles, please see Section 3.2 for diurnal profiles of nitrate-containing particles.

As shown in Fig. 2, most of particle types were in the droplet mode. ECOC-Sul, ECOC-Sul-Nit, and OC were predominant in the size range <0.7 μm. These particle types are all traffic-related (please see Section 3.2). The unscaled size distributions of ECOC-Sul and ECOC-Sul-Nit were consistent with previous studies (Sodeman et al., 2005; Toner et al., 2008; Toner et al., 2006). However, when D_{va} > 0.7 μm, EC-Nit and EC-Sul-Nit were major particle types. This pattern was unique because EC related particles commonly peaked with D_{va} < 0.7 μm (Dall'osto and Harrison, 2006; Moffet et al., 2008; Pratt and Prather, 2009). Meanwhile, the fresh EC particles peaked at 0.5 μm, EC-Nit and EC-Sul-Nit peaked at 0.72 and 0.74 μm, respectively. One explanation for is that, due to the uptake of oxidized organic species, sulfate, and nitrate on the EC-related particles, their size distribution shifted towards the larger size rapidly in the aging process (Moffet and Prather, 2009).

3.2. Source and origination of urban particles

Time series of temperature (Temp), relative humidity (RH), wind speed (WS), wind direction (WD), gases (SO_2 and O_3, NO_2 and NO), $PM_{2.5}$ and SPAMS count are shown in Fig. 3. The average concentrations of $PM_{2.5}$, NO, O_2, SO_2, and O_3 were 59 ± 7 μg m^{-3}, 10 ± 3 μg m^{-3}, 44 ± 5 μg m^{-3}, 13 ± 2 μg m^{-3}, 61 ± 8 μg m^{-3}, respectively.

During the sampling period, wind was mainly from the southeast (35%), northeast (21%), and east (13%, Fig. S4). When wind speed was lower than 1.5 m s^{-1}, it was typically considered as stagnant air condition (Huang et al., 2017), which took up to 82% of wind cases. In these conditions, the distance of PM transport would be limited. Therefore, ambient particles in sampling site were controlled by local emissions from residential communities and nearby traffic, as well as pollutants from the southeast part of the city.

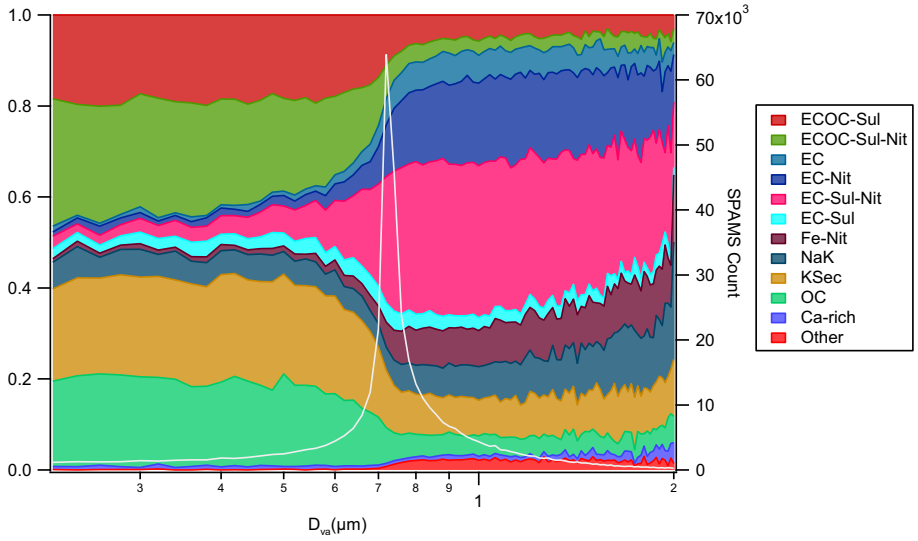

Fig. 2. Unscaled size distribution of particle types (left) and the total size bin of SPAMS raw counts in the dataset (right), indicated by the white curve.

In order to understand the source and origination of urban particles, a wind-dependent analysis was conducted. Correspondingly, the correlations between pollutants is shown in Table 1. Two types of origination were identified, including local emission and regional transport (Fig. 4). NO, and NO_2 were pronounced locally under stagnant air conditions (wind speed < 1.5 m s^{-1}); the similar wind-dependent behavior was found in ECOC-Sul-Nit (R = 0.61 with NO), Ca-Nit (R = 0.68 with NO_2), and NaK-Nit (R = 0.69 with NO). In addition, ECOC-Sul also had good correlation with NO (R = 0.71). Judging from its wind-dependent plot, ECOC-Sul was from locally aging and the south. As described above, the sampling site is surrounded by city roads (1 km away) and ring-shaped highways (3 km away). Diurnal pattern of these particle types were also shown in Fig. 5. As expected, they all had similar profiles which were indicated by the 4:00 and 9:00 peaks. According to the local traffic regulation, heavy-duty trucks were only allowed to enter the urban area between 0:00 and 6:00. Therefore the

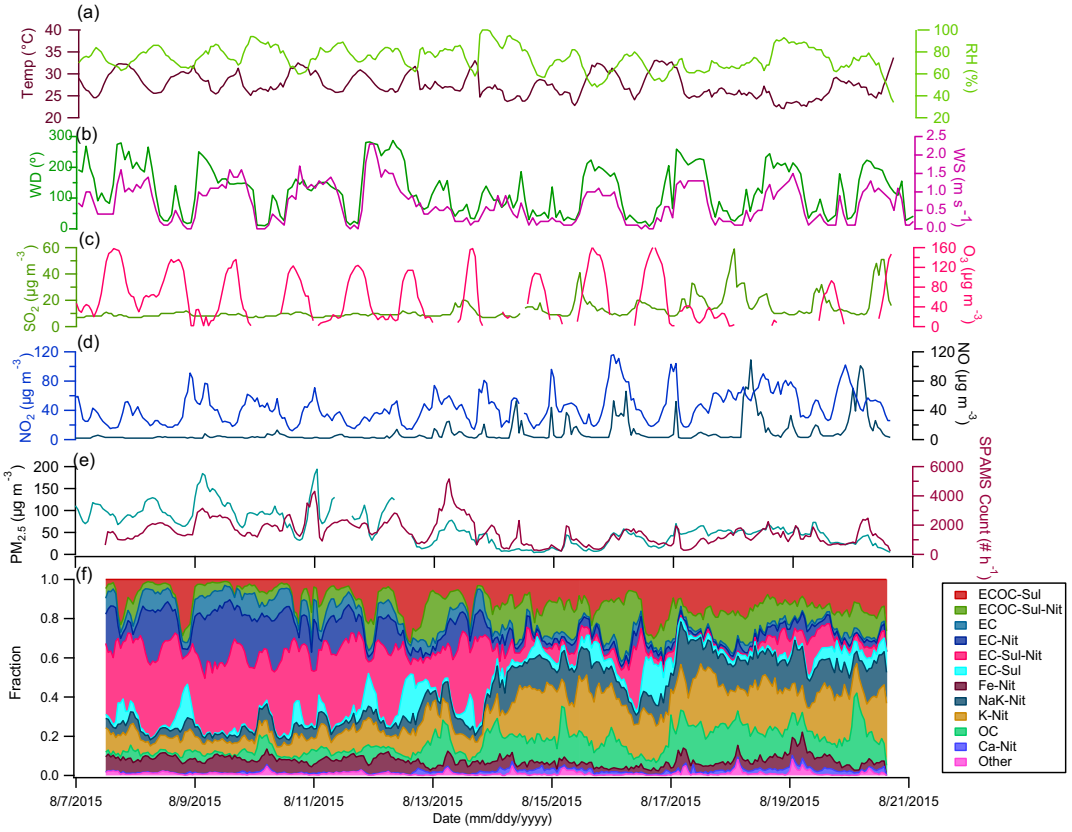

Fig. 3. Time series of (a) temperature and relative humidity (RH); (b) wind speed (WS) and direction (WD); (c) SO_2 and Ozone; (d)NO_2 and NO; (e) $PM_{2.5}$ and SPAMS count per hour; and (f) number fraction of SPAMS particle types.

Table 1
Correlations between gaseous pollutants and hourly count of particle types.

	NO	NO_2	SO_2	CO	O_x[a]
ECOC-Sul	0.71	0.34	0.21	0.12	0.16
EC	0.26	0.23	−0.20	0.68	−0.21
EC-Nit	−0.04	0.16	−0.15	0.53	−0.17
EC-Sul-Nit	−0.05	0.13	−0.01	0.40	−0.03
EC-Sul	−0.07	−0.23	0.36	−0.10	0.68
Fe-Nit	0.04	0.08	−0.06	0.66	0.64
NaK	0.69	0.58	0.04	0.36	−0.36
K-Nit	0.28	0.50	0.11	0.30	−0.17
ECOC-Sul-Nit	0.60	0.47	−0.18	0.27	−0.42
OC	0.30	0.26	−0.15	0.66	−0.37
Ca-Nit	0.53	0.68	−0.15	0.21	−0.45
NO	1.00	0.34	0.00	0.70	−0.23
NO_2ppb		1.00	−0.30	0.64	−0.52
SO_2			1.00	−0.20	0.35
CO				1.00	−0.17
O_x					1.00

[a] Unit of Gases is μg m^{-3}, and unit of particle type is count h^{-1}.

4:00 peak of NO were typically from these heavy-duty vehicles. In addition, Fe-Nit, NaK-Nit, and Ca-Nit particles, commonly recognized as dust-related types (Chen et al., 2016), showed similar diurnal patterns to NO, suggesting that they were possibly loft into the atmosphere due to traffic activities in the highway.

The busiest highway hub (near the label "S311" on Fig. 2) is located in the southeast of the sampling site. As expected, wind from southeast brought pollutants to the sampling site and caused the $PM_{2.5}$ elevating. Similar patterns were also found in wind-dependent plots of O_x, EC, EC-Nit, EC-Sul-Nit, and Fe-Nit (Fig. 6). In typical urban areas, CO is mainly from traffic emissions. The wind-dependent plot of CO suggested that it was pronounced when either air was stagnant, or the wind blew from the southeast. Fe-Nit had a profile of dust components resuspended on the road (Zhang et al., 2014). CO had good correlations with EC (R = 0.68), Fe-Nit (0.66). OC particles were also well correlated with CO (R = 0.66), but its diurnal pattern is more similar with NO, and wind-dependent plots also suggest that it was influenced by the local emissions and southeast wind. According to the Statistical Yearbook of Xi'an, there are the 2.22 million gasoline-powered vehicles, and 0.23 million diesel-power vehicles. Although heavy-duty vehicles are not allowed to enter the urban area which is defined by the inside of G65 in the North during daytime (6:00–22:00). The influence of heavy-duty vehicles on G65 was inevitable because the sampling site is 3 km away. NO and NO_2 concentrations were majorly influenced by heavy-duty diesel trucks, with the obvious early morning peak around 4:00, when it is unlikely for a large number of gasoline-powered automobiles being on the road. Thus, the OC particle type had weak correlations with NO and NO_2, and OC particles were more likely from light-duty vehicles and gasoline-powered automobiles.

The diurnal plots of gaseous pollutant and particle type mentioned above are shown in Fig. 7. EC, EC-Nit, OC, and Fe-Nit had clear morning peak around 7:00. EC-Nit, EC-Sul, and Fe-Nit also had noon peaks around 12:00–14:00, indicating the influence of strong photochemical activities. In addition, EC-Sul and EC-Nit were well correlated with O_x (R = 0.64 and 0.68, respectively).

SO_2 was majorly from the west where a power plant is located. After leaving the plume, SO_2 encountered fresh EC particles from the southeast and formed EC-Sul in the southwest and south of the sampling site (Fig. S5). This result suggests that chemical composition of urban particles strongly depends on their transport routes. EC-Sul also peaked in the early morning (4:00) but were more pronounced at noon due to photochemical activities. In a tunnel study, Gross et al. (2000b) reported single particle mass spectra of PAH- and EC-containing particles in which sulfate was found. More directly, Toner et al. (2006) reported single particle mass spectra of exhaust samples from five heavy-duty diesel trucks, the primary sulfate was observed with a minor fraction. In a

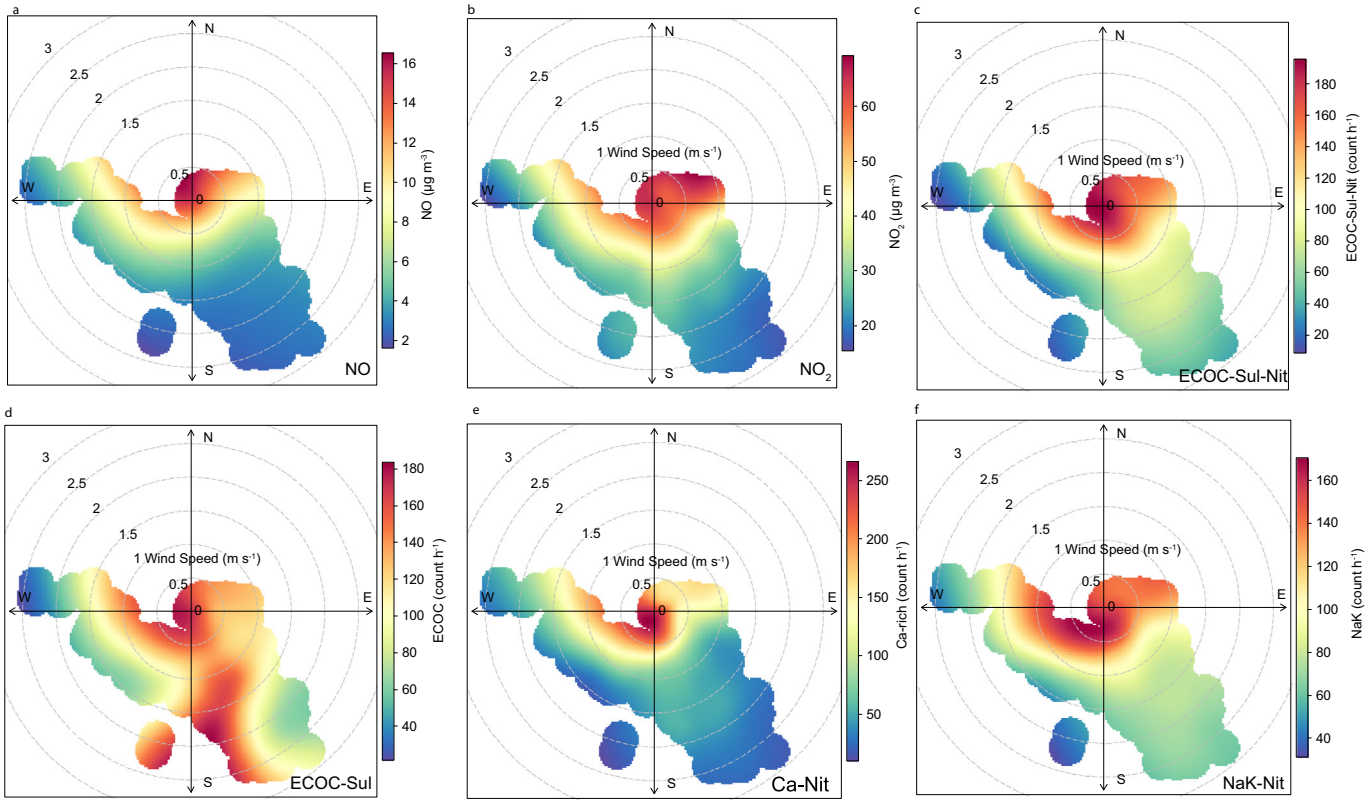

Fig. 4. Bivariate polar plots of (a) NO, (b)NO_2, (c) ECOC-Sul-Nit, (d) ECOC-Sul, (e) Ca-Nit, and (f) NaK-Nit. These plots were developed by the method from Carslaw et al. (2006).

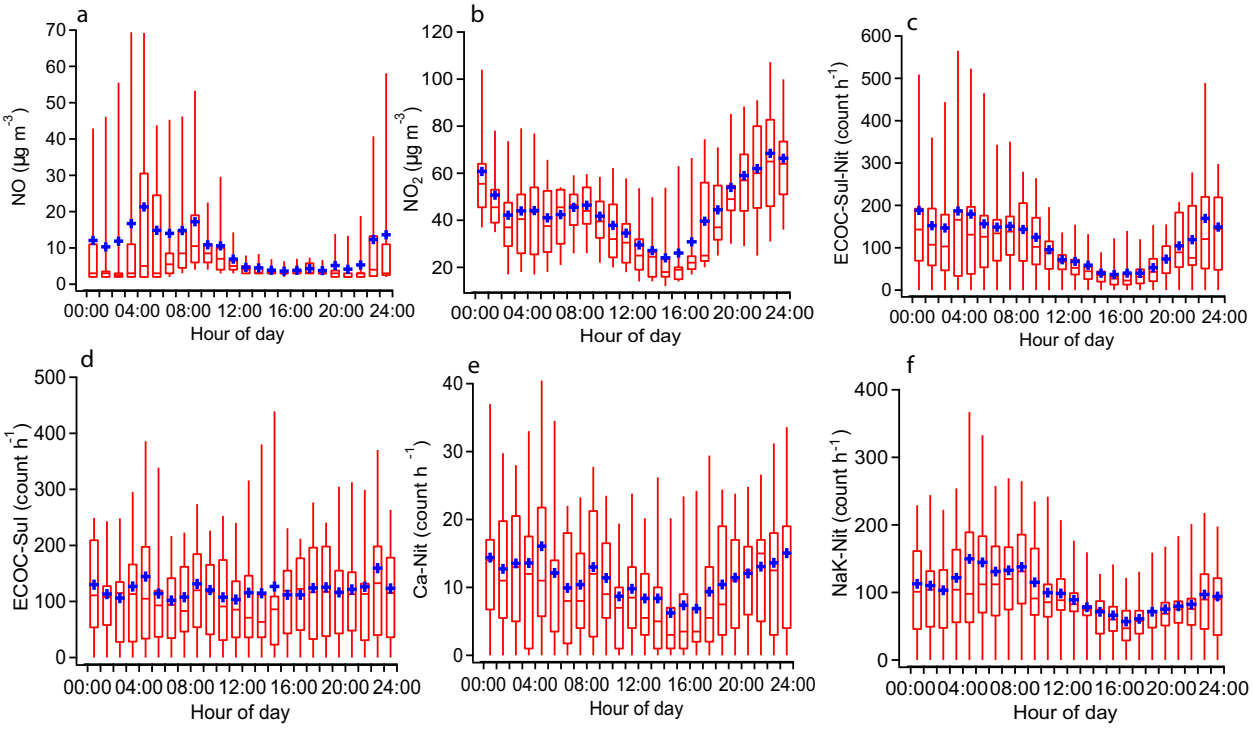

Fig. 5. Diurnal plots of (a) NO, (b) NO_2, (c) ECOC-Sul-Nit, (d) ECOC-Sul, (e) Ca-Nit, and (f) NaK-Nit. Blue cross indicates the mean value of each box, and the box indicates the 25th and 75th percentiles, the ends of lines are 10th and 90th percentiles.

study of diesel exhaust using scanning electron microscopy, the presence of sulfate from diesel engine exhaust was also present (Liati et al., 2013). There were also some reports about the primary sulfate in diesel exhaust (Biswas et al., 2009; Suess and Prather, 2002). Therefore, we proposed that the weak peak of EC-Sul occur at 4 a.m. was from the direct emission of diesel engine exhaust rather than the secondary formation. However, the noon peak of EC-Sul was possibly secondary. In addition, K-Nit was recognized as a regional, mainly from the east (Fig. S6).

Conclusively, the EC family, ECOC-Sul-Nit, ECOC-Sul, Ca-Nit, Fe-Nit, and OC were all traffic-related. EC family, OC, and Fe-Nit were mainly from the Southeast; Ca-Nit, ECOC-Sul, and ECOC-Nit were locally emitted.

3.3. Aerosol acidity

The relative aerosol acidity is defined as:

$$\text{relative aerosol acidity} = (\text{sulfate} + \text{nitrate})/\text{ammonium} \quad (1)$$

where sulfate, nitrate, and ammonium are peak areas of nitrate (m/z −62), sulfate (m/z −97), and ammonium (m/z 18), respectively. The relative aerosol acidity has been used to evaluate relative aerosol acidity in single particle mass spectrometry (Denkenberger et al., 2007; Huang et al., 2013; Yao et al., 2011). There are several points to be noted. This method is substantially mass-based. When SPAMS processing different size or chemical composition particles, due to variations of size-dependent transmission efficiencies, hit rate, and efficiency of data acquisition, quantitive number concentration of ambient particle is difficult to be achieved only using SPAMS (Healy et al., 2012; Pratt and Prather, 2012). A particle sizer will be useful to scaling SPAMS dataset to real ambient particles via correction of transmitting efficiencies. Numerous studies have been proved that distribution of chemical species is size-dependent (Pratt and Prather, 2012). Matrix effect has been observed in single particle mass spectrometer studies (Dall'osto and Harrison, 2006; Gross et al., 2000a). Therefore, uncertainty of this estimation should be considered. Huang et al. (2013) reported a good correlation between the ATOFMS relative acidity evaluation with the mass-based technology and a good agreement had been acquired (Huang et al., 2013). The size-dependent acidity is shown in Fig. 8a, the highest acidity occurred with a size range <200 nm, then the acidity decreased and tended to be stable in the supermicron mode. In this study, peak area of sulfate, nitrate, and ammonium with a size range 0.2–1.4 μm, in which covered 96% of collected particles, were extracted for aerosol acidity evaluation.

The time series of relative acidity and $PM_{2.5}$ could be separated into two stages (Fig. 8e). From 08/08 to 08/14, wind mostly blew from the southeast at speed between 1.5 and 3 m s^{-1}; while during period from 08/14 to 08/21, wind blew from all directions at speed of lower than 2 m s^{-1}. During these two periods, the relative aerosol acidity became stronger after 08/14, when it was under a more severe air stagnant condition (Fig. 8c). Relative acidity showed a rising trend when EC-Sul-Nit and EC-Nit decreased dramatically. The increased particle types, such as OC, ECOC-Sul-Nit, and K-Nit were more acidic (Fig. 8b). Aerosol acidity would increase because of the uptake of acidic gases such as HCl, HNO_3, and H_2SO_4 after particles were emitted from the plume. It would take from hours to days for the aerosol acidity decreasing when these freshly-emitted particles were neutralized by the ambient NH_3 and other alkalic species during aging (Yao et al., 2011). Therefore, the variation of relative aerosol acidity could be used as an indicator of aerosol aging. In the period from 08/08 to 08/14, the wind speed was high, and less acidic particles were brought. However, during 08/14 to 08/21, a $PM_{2.5}$ mass accumulation event occurred (Fig. 8e) with stronger aerosol acidity, indicating that the less-aged particles formed under stagnant air conditions.

Fig. 9 shows diurnal profiles of relative acidity of urban aerosols during summertime. In summertime, the highest relative acidity occurred at 7:00 in the morning, with an average value of 55; while the lowest value (23) appeared at 15:00 in the afternoon. It implies that the fresh particles were more acidic in Xi'an. In addition, producing of H_2SO_4

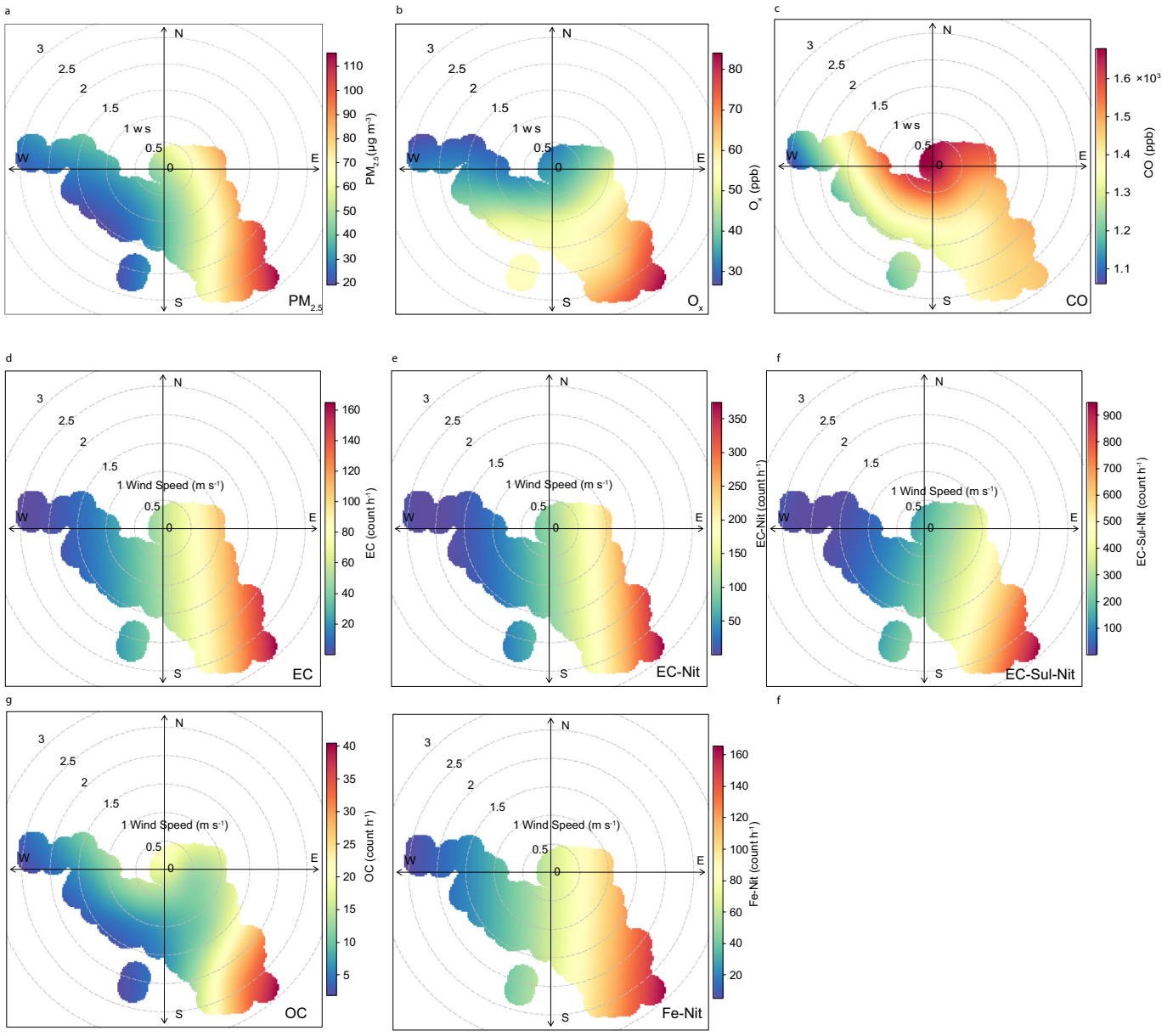

Fig. 6. Bivariate polar plots of (a) $PM_{2.5}$, (b) O_x, (c) CO, (d) EC, (e) EC-Nit, (f) EC-Nit-Sul, (g) OC, and (h) Fe-Nit. The plots were developed by the method from Carslaw et al. (2006).

and HNO_3 in the aerosol droplets were the major sources of aerosol acidity in the early morning. The aqueous formation of HNO_3 (a) is mainly via OH+ NO_2 and peroxides+ NO_2 reaction homogenously under the solar radiation (Zhang et al., 2015). However, the formation of H_2SO_4 is more complicated. There are several pathways could cause rapid formation of sulfate via heterogeneous reactions or in the aerosol droplet. For example, He et al. (2014) proposed that SO_2 and NO_2 can rapidly react with each other on the surface of dust, leading to the rapid formation of sulfate. With presence of Fe and Mn in the particle phase, OH radical, H_2O_2 or organic peroxides could be generated via Fenton reaction as the drive to oxidize S(IV) to H_2SO_4 (Barbusinski, 2009). Moreover, aerosol water could act as a reactor where SO_2 could be oxidized by NO_2 when the atmospheric neutralizing capacity is high (Cheng et al., 2016). At noon, HNO_3 which formed from the reaction of acidic gases and NH_4NO_3 enters the gas phase, and uptake of ammonium resulting in decrease of relative aerosol acidity (Yao et al., 2011).

Box plot of relative aerosol acidity at various RH is shown in Fig. 9b. When RH increased from 40 to 70%, the relative aerosol acidity decreased from 39 to 25 due to the increase of aerosol water content when RH elevated. When RH > 80%, the size-dependent aerosol acidity kept increasing up to a mean value of 55. It was possible that, with sufficient acidic substance, the relative aerosol acidity kept increasing in the urban area of Xi'an. Moreover, our trend disagreed with Huang et al. (2013) reported that aerosol acidity peaked in the afternoon. This relationship of aerosol acidity and RH was inconsistent with Zhou et al. (2012) reported in a mountainous area. Zhou et al. (2012) proposed that, in a high mountain site, the highest aerosol acidity occurred when RH was in a range of 50–70%, then aerosol acidity decreased because of the dilution of more aerosol water content when RH > 70%. However, in this study, with sufficient acidic gases in the urban area (Through the whole 08/2015, the gaseous HCl was 0.09 ± 0.06 μg m^{-3}, HONO 4.2 ± 2.4 μg m^{-3}, HNO_3 1.80 ± 1.0 μg m^{-3}, and H_2SO_4 0.9 ± 0.4 μg m^{-3}, data not published), the relative acid kept increasing with elevating RH.

Qualitatively, the relationship between aerosol water content and aerosol acidity is complicated. Aerosol acidity is determined by the concentration of H^+ ($[H^+]$) in the aerosol water. $[H^+]$ is majorly

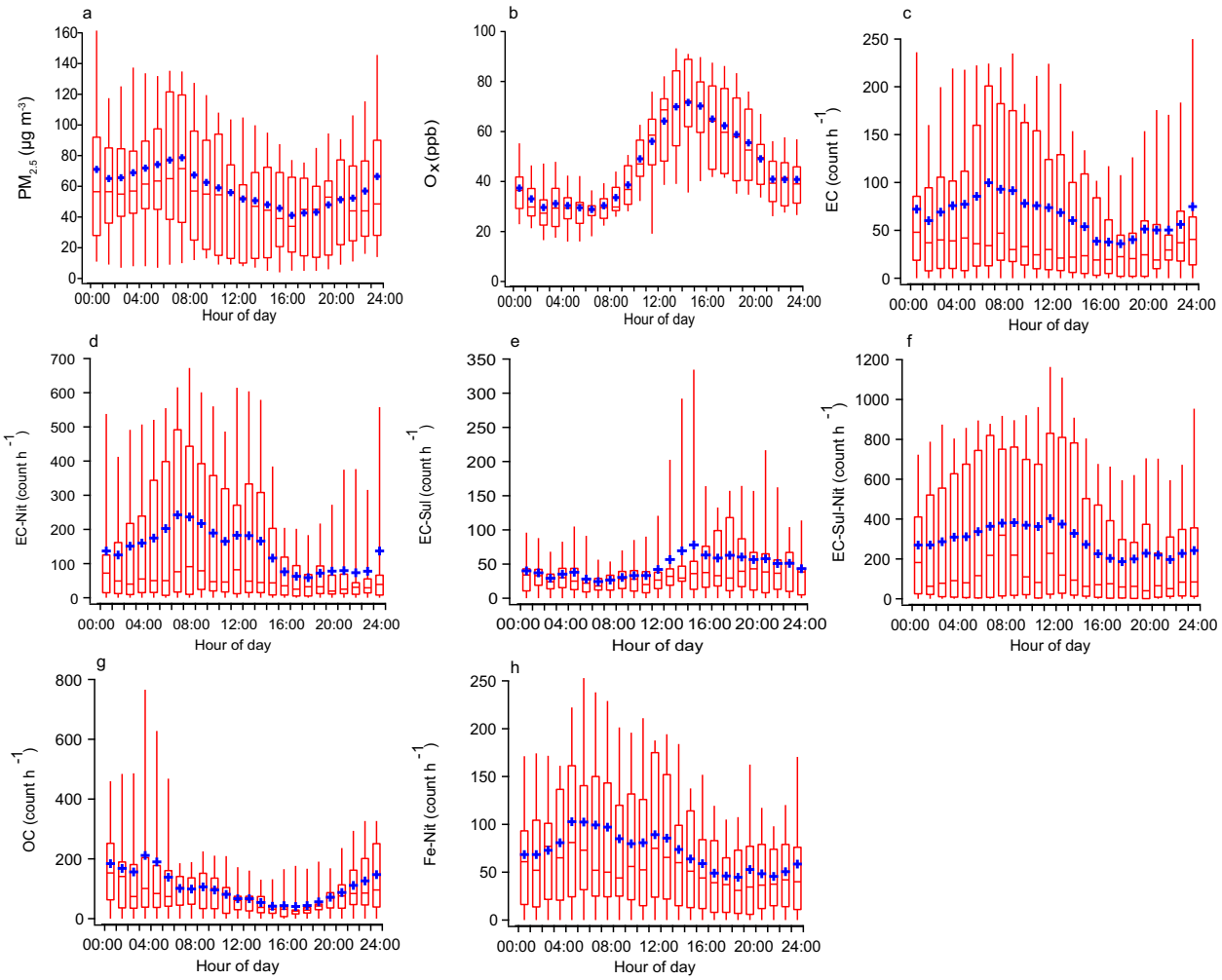

Fig. 7. Diurnal plots of (a) $PM_{2.5}$, (b) O_x, (c) CO, (d) EC, (e) EC-Nit, (f) EC-Nit-Sul, (g) OC, and (h) Fe-Nit. Blue cross indicates the mean value of each box, and box indicates the 25th and 75th percentiles, ends of line on the box are 10th and 90th percentiles.

determined by the concentration of SO_4^{2-}, NO_3^-, and NH_4^+ (Pathak et al., 2004). These hygroscopic species can retain water at low RH and provide substances for water uptake thus increases aerosol water content (Khlystov et al., 2005). The elevating water content can enhance the uptake of species like SO_2, H_2SO_4, and HNO_3 due to the larger aerosol surface (Seinfeld and Pandis, 2012). The uptake of acidic species such as SO_2, H_2SO_4, HCl, and HNO_3 can increase aerosol acidity, especially when Fe^{2+} and other transition metal co-exist with H_2O_2 for Fenton reaction to provide OH radical for the aqueous oxidation of SO_2 to H_2SO_4 (Zhang et al., 2015). In these terms, an increase of water content would whether increase or decrease aerosol acidity is difficult to determine. Besides, the non-catalytic SO_2 oxidation in the presence of NH_3 is considerable when RH 75–80% (Turšič et al., 2004). It might be another reason for the elevating of aerosol acidity when RH was high.

3.4. Mixing state of Secondary Organic Aerosol (SOA) markers

Mixing state of a particle refers to how chemical species are distributed among the particles present in an aerosol population (Healy et al., 2014). Qin et al. (2012) proposed that m/z 43 ($C_2H_3O^+$) represented an appropriate ATOFMS marker for secondary oxidized organic species or SOA. Moreover, $C_2H_3O^+$ fragment is commonly a marker for ketones and aldehydes (Hawkins and Russell, 2010), which can undergo gas-to-particle phase partitioning to form SOA (Hallquist et al., 2009; Odum et al., 1997). Oxalic acid (m/z −89) is used as a marker for aqueous SOA (Carlton et al., 2007; Ervens et al., 2011), but sometimes as a marker for biomass burning (Falkovich et al., 2005). Given that a marker is widely found in the major particle types with considerable ratios and ion intensities, it is reasonable to deduce that the certain pathway of SOA formation is important for that particle type.

As shown in the top panel of Fig. 10, $C_2H_3O^+$ had high fractions in OC related particles, such as 86% of OC, 81% of ECOC-Sul-Nit, 55% of ECOC-Sul; meanwhile it had low fraction in EC-related particles, such as 6% in EC-Nit, 8% in EC-Sul-Nit, 11% in EC, and 36% in EC-Sul, and median fraction in other particle types such as Fe-Nit (24%), Ca-Nit (31%), NaK (35%), and K-Nit (42%). In the mixing intensity view, OC had the highest mixing intensity of $C_2H_3O^+$ (0.10), followed by ECOC-Sul-Nit (0.034) and Ca-Nit (0.023). SOA formation via gas phase include gas-to-particle phase partitioning and coagulation of organic aerosols (Robinson et al., 2013); in these processes, primary organic aerosol (POA) and associated semi-volatile vapors can play an important role in the formation of SOA (Robinson et al., 2007). If SOA and POA are miscible, POA would enhance SOA formation (Vaden et al., 2010). In this case, such dramatic discrepancies on mixing ratio and intensity of $C_2H_3O^+$ suggested that photooxidation and gas-to-particle phase partitioning were unlikely the only pathway for SOA formation. We also found that secondary organic species intend to uptake on the OC-related particles such as OC, ECOC-Sul-Nit and ECOC-Sul, suggesting that mass transfer or diffusion limitations are favorable for POA vapors' uptake on OC-related types. Indeed, photooxidation of organic species

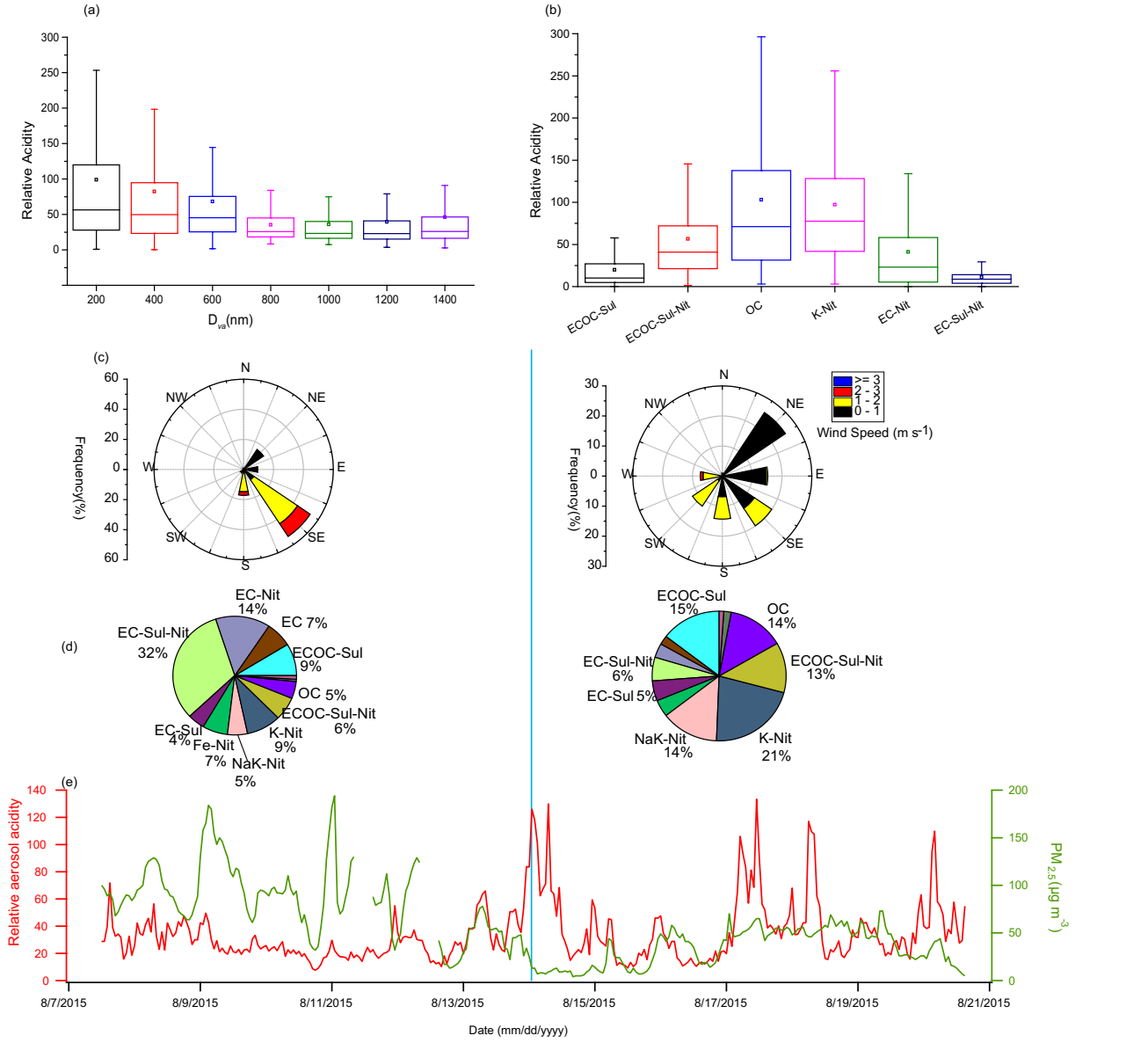

Fig. 8. (a) Box plots of size-dependent aerosol acidity (D_{va}); (b) box plots of type-specific aerosol acidity; (c) wind rose plots of 08/08/2015–08/14/2015 (left) and 08/14/2015–08/21/2015 (right); (d) pie charts of particle type fraction from 08/08/2015–08/14/2015 (left) and 08/15/2015–08/21/2015 (right); (e) time series of relative aerosol acidity (red) and $PM_{2.5}$ concentration (green).

when reacting with OH radical on the surface of aerosol can also generate SOA, but this process is not as rapid as the gas phase processes (McNeill, 2014).

Oxalate is commonly used as a tracer for aqueous SOA (Ortiz-Montalvo et al., 2012). However, in studies of Shanghai and Shenzhen, which are both southern cities in China, contribution of biomass burning could not be excluded (Huang et al., 2006; Yang et al., 2009). In this study, Oxalate had much lower mixing ratios (one magnitude) than $C_2H_3O^+$. For example, Oxalate was only determined in 9% of OC, 7% of Fe-Nit, and 6% in K-Nit particle types. The highest mixing ratio and relative intensity of oxalate were found in the OC type, which were 10% and 8.5×10^{-4}, respectively. The OC type contained weak ion fragments such as m/z −45, −59 and −71, which were markers of levoglucosan. As described in Section 3.2, the OC type was mainly from traffic, but their coagulation with biomass burning particle was also observed. Well known that POA from traffic are hydrophobic (Canagaratna et al., 2004), but the presence of hygroscopic species is able to retain aerosol water at low RH (Khlystov et al., 2005) to maintain particles in droplet where the formation of oxalate due to oxidation of glyoxal is applicable (Ervens et al., 2011). NaK also contained a high ratio of oxalate, possible due to the contribution of primary oxalate from biomass burning (Falkovich et al., 2005). Interestingly, although Fe-Nit was not rich in organic species, the high mixing ratio of oxalate (9%) and relatively strong (5.5×10^{-4}) in Fe-Nit indicating that the aqueous oxidation of glyoxal from OH radical was important when Fe (II) present as a catalyst of Fenton Reaction to produce OH radical (Ervens et al., 2011). Although the enhancing of oxalate has been observed, but there are several points should be noted: 1) the Photo-Fenton process is complicated, it is difficult to evaluate the effect of the process without quantitative measurement; 2) the Photo-Fenton process contained not only the OH production catalyzed by Fe(II), and the photodecomposition of Fe(III)-oxalate complexes, the latter is controlled by pH and irradiation (Kim and Vogelpohl, 1999). Therefore, in Fe-Nit, the production and decomposition of oxalate co-existed. Although the photochemical decomposition of oxalate is fast in the order of a few minutes whenever the concentration of dissolved iron

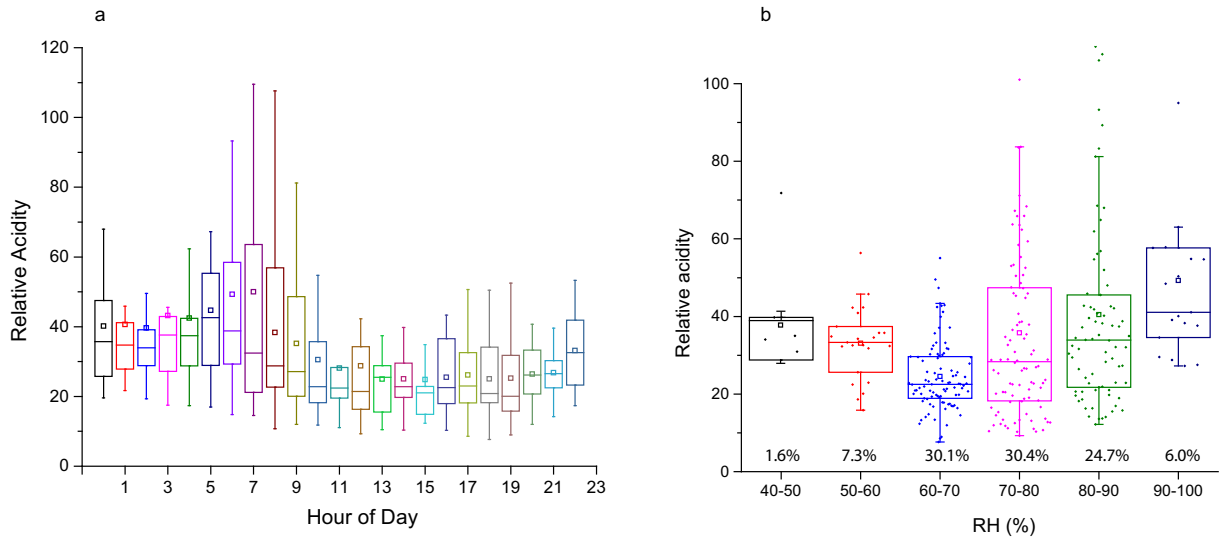

Fig. 9. a. Diurnal variations of relative aerosol acidity box plots in summer. Mean (square), median (middle horizontal line), 25th and 75th percentiles (P25–P75, box) and 10th and 90th percentiles (P10–P90, whiskers) are displayed; b. Box plot of relative aerosol acidity as a function of RH. Mean (square), median (middle horizontal line), 25th and 75th percentiles (P25–P75, box) and 10th and 90th percentiles (P10–P90, whiskers) are reported for each RH bin (10% per step). The percentages below each number are the population size of each box plot.

(III) is comparable to that of the organic acids (Zuo and Hoigné, 1994); still, the production of oxalate should be more significant for its accumulation in Fe-Nit.

In summary, both m/z 43 and −89 were found in major particle types, but the mixing ratios and intensities of m/z 43 were one-magnitude higher than that of m/z −89. Although SPAMS cannot provide quantitative meaning of SOA formation, the formation behaviors on each particle type can be obtained. Conclusively, semi-volatile vapors are favorable to condense on the OC-related particles possibly due to mass transfer barriers or diffusion limitations; oxalate also tends to be formed in the droplet of OC-related particles via heterogeneous reactions.

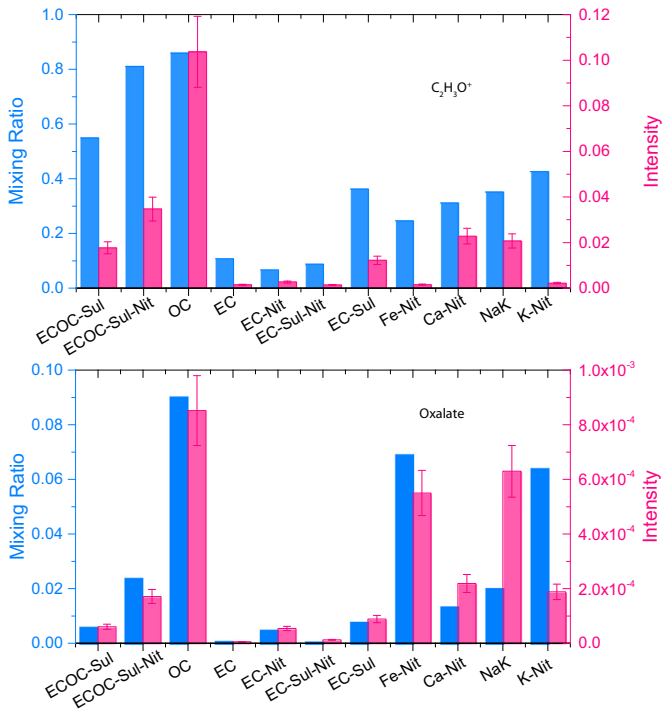

Fig. 10. Top panel: Mixing ratio (the ratio of a particle type containing the certain markers) of $C_2H_3O^+$ (m/z 43, blue) and averaged relative intensity of m/z 43 (pink) in each particle type; Bottom Panel: Mixing ratio of oxalate (m/z −89, blue) and averaged relative intensity of −89 (pink) in each particle type.

4. Conclusions

Size-resolved chemical composition and mixing state of urban particles were investigated in Xi'an during summertime. Chemical composition, diurnal plot and wind dependent analysis suggested that up to 83% of the particles were traffic-related. Two major originates of particles, including aging in stagnant and transport from the southeast, were identified. The size-dependent aerosol acidity was evaluated, particles with smaller diameter were more acidic, and the relative acidity was found peaking between 7:00–9:00 when RH 60–70%. Semi-volatile vapors are favorable to condense on OC-related particles possibly due to mass transfer barriers or diffusion limitations; oxalate also tends to be formed in the droplet of OC-related particles. In Fe-Nit particles, enrichment of oxalate was also observed. This study provides an evaluation of major particle types, chemical composition, source, and origination of urban particles in Xi'an. This study also contributed a new understanding of characterization, process, and behavior of urban particles in the urban areas of Guanzhong Basin, Northwestern China.

Acknowledgments

Financial support from Nature Science Foundation of China (Grant No. 41375123), "Western Talents" of Chinese Academy of Sciences, Chongqing Science and Technology Commission (Grant No. cstc2015jcyjA20003), the National Key R&D Program of China (2016YFC0200400), and the project from Ministry of Science and Technology (2013FY112700) are acknowledged.

Appendix A. Supplementary data

Supplementary data to this article can be found online at https://doi.org/10.1016/j.scitotenv.2018.04.388.

References

Barbusinski, K., 2009. Fenton reaction - controversy concerning the chemistry. Ecological Chemistry and Engineering S-chemia I Inzynieria Ekologiczna S, pp. 347–358.
Bei, N., Xiao, B., Meng, N., Feng, T., 2016. Critical role of meteorological conditions in a persistent haze episode in the Guanzhong basin, China. Sci. Total Environ. 550, 273–284.

Biswas, S., Verma, V., Schauer, J.J., Sioutas, C., 2009. Chemical speciation of PM emissions from heavy-duty diesel vehicles equipped with diesel particulate filter (DPF) and selective catalytic reduction (SCR) retrofits. Atmos. Environ. 43, 1917–1925.

Canagaratna, M.R., Jayne, J.T., Ghertner, D.A., Herndon, S.C., Shi, Q., Jimenez, J.L., et al., 2004. Chase studies of particulate emissions from in-use New York City vehicles. Aerosol Sci. Technol. 38, 555–573.

Cao, J., 2014. $PM_{2.5}$ and Environment in China. Science Press, Beijing.

Cao, J.J., Chow, J.C., Watson, J.G., Wu, F., Han, Y.M., Jin, Z., et al., 2008. Size-differentiated source profiles for fugitive dust in the Chinese Loess Plateau. Atmos. Environ. 42.

Cao, J.J., Zhu, C.S., Tie, X.X., Geng, F.H., Xu, H.M., Ho, S.S.H., et al., 2012. Characteristics and sources of carbonaceous aerosols from Shanghai, China. Atmos. Chem. Phys. Discuss. 12, 16811–16849.

Carlton, A.G., Turpin, B.J., Altieri, K.E., Seitzinger, S., Reff, A., Lim, H.-J., et al., 2007. Atmospheric oxalic acid and SOA production from glyoxal: results of aqueous photooxidation experiments. Atmos. Environ. 41, 7588–7602.

Carslaw, D.C., Beevers, S.D., Ropkins, K., Bell, M.C., 2006. Detecting and quantifying aircraft and other on-airport contributions to ambient nitrogen oxides in the vicinity of a large international airport. Atmos. Environ. 40, 5424–5434.

Chen, W.T., Shao, M., Lu, S.H., Wang, M., Zeng, L.M., Yuan, B., et al., 2014. Understanding primary and secondary sources of ambient carbonyl compounds in Beijing using the PMF model. Atmos. Chem. Phys. 14, 3047–3062.

Chen, Y., Cao, J., Huang, R., Yang, F., Wang, Q., Wang, Y., 2016. Characterization, mixing state, and evolution of urban single particles in Xi'an (China) during wintertime haze days. Sci. Total Environ. 573, 937–945.

Chen, Y., Wenger, J.C., Yang, F., Cao, J., Huang, R., Shi, G., et al., 2017. Source characterization of urban particles from meat smoking activities in Chongqing, China using single particle aerosol mass spectrometry. Environ. Pollut. 228, 92–101.

Cheng, Y., Zheng, G., Wei, C., Mu, Q., Zheng, B., Wang, Z., et al., 2016. Reactive nitrogen chemistry in aerosol water as a source of sulfate during haze events in China. Sci. Adv. 2.

Dall'osto, M., Harrison, R., 2006. Chemical characterisation of single airborne particles in Athens (Greece) by ATOFMS. Atmos. Environ. 40, 7614–7631.

Denkenberger, K.A., Moffet, R.C., Holecek, J.C., Rebotier, T.P., Prather, K.A., 2007. Real-time, single-particle measurements of oligomers in aged ambient aerosol particles. Environ. Sci. Technol. 41, 5439–5446.

Ervens, B., Turpin, B.J., Weber, R.J., 2011. Secondary organic aerosol formation in cloud droplets and aqueous particles (aqSOA): a review of laboratory, field and model studies. Atmos. Chem. Phys. 11, 11069–11102.

Falkovich, A.H., Graber, E.R., Schkolnik, G., Rudich, Y., Maenhaut, W., Artaxo, P., 2005. Low molecular weight organic acids in aerosol particles from Rondonia, Brazil, during the biomass-burning, transition and wet periods. Atmos. Chem. Phys. 5, 781–797.

Gross, D.S., Galli, M.E., Silva, P.J., Prather, K.A., 2000a. Relative sensitivity factors for alkali metal and ammonium cations in single-particle aerosol time-of-flight mass spectra. Anal. Chem. 72, 416–422.

Gross, D.S., Galli, M.E., Silva, P.J., Wood, S.H., Liu, D.-Y., Prather, K.A., 2000b. Single particle characterization of automobile and diesel truck emissions in the Caldecott Tunnel. Aerosol Sci. Technol. 32, 152–163.

Hallquist, M., Wenger, J.C., Baltensperger, U., Rudich, Y., Simpson, D., Claeys, M., et al., 2009. The formation, properties and impact of secondary organic aerosol: current and emerging issues. Atmos. Chem. Phys. 9, 5155–5236.

Hawkins, L.N., Russell, L.M., 2010. Oxidation of ketone groups in transported biomass burning aerosol from the 2008 Northern California Lightning Series fires. Atmos. Environ. 44, 4142–4154.

He, H., Wang, Y., Ma, Q., et al., 2014. Mineral dust and NOx promote the conversion of SO_2 to sulfate in heavy pollution days. Sci. Rep. 4, 4172.

Healy, R.M., Hellebust, S., Kourtchev, I., Allanic, A., O'Connor, I.P., Bell, J.M., et al., 2010. Source apportionment of $PM_{2.5}$ in Cork Harbour, Ireland using a combination of single particle mass spectrometry and quantitative semi-continuous measurements. Atmos. Chem. Phys. 10, 9593–9613.

Healy, R.M., Sciare, J., Poulain, L., Kamili, K., Merkel, M., Müller, T., et al., 2012. Sources and mixing state of size-resolved elemental carbon particles in a European megacity: Paris. Atmos. Chem. Phys. 12, 1681–1700.

Healy, R.M., Riemer, N., Wenger, J.C., Murphy, M., West, M., Poulain, L., et al., 2014. Single particle diversity and mixing state measurements. Atmos. Chem. Phys. 14, 6289–6299.

Huang, X., Yu, J.Z., He, L., Yuan, Z., 2006. Water-soluble organic carbon and oxalate in aerosols at a coastal urban site in China: size distribution characteristics, sources, and formation mechanisms. J. Geophys. Res. 111.

Huang, Y., Li, L., Li, J., Wang, X., Chen, H., Chen, J., et al., 2013. A case study of the highly time-resolved evolution of aerosol chemical and optical properties in urban Shanghai, China. Atmos. Chem. Phys. 13, 3931–3944.

Huang, R.-J., Zhang, Y., Bozzetti, C., Ho, K.-F., Cao, J.-J., Han, Y., et al., 2014. High secondary aerosol contribution to particulate pollution during haze events in China. Nature 514, 218–222.

Huang, Q., Cai, X., Song, Y., Zhu, T., 2017. Air stagnation in China (1985–2014): climatological mean features and trends. Atmos. Chem. Phys. 17, 7793–7805.

Khlystov, A., Stanier, C.O., Takahama, S., Pandis, S.N., 2005. Water content of ambient aerosol during the Pittsburgh Air Quality Study. J. Geophys. Res. 110.

Kim, S.M., Vogelpohl, A., 1999. Degradation of organic pollutants by the photo-fenton-process. Chem. Eng. Technol. 21, 187–191.

Li, L., Huang, Z., Dong, J., Li, M., Gao, W., Nian, H., et al., 2011. Real time bipolar time-of-flight mass spectrometer for analyzing single aerosol particles. Int. J. Mass Spectrom. 303, 118–124.

Li, N., Long, X., Tie, X., Cao, J., Huang, R., Zhang, R., et al., 2016. Urban dust in the Guanzhong basin of China, part II: a case study of urban dust pollution using the WRF-Dust model. Sci. Total Environ. 541, 1614–1624.

Liati, A., Schreiber, D., Dimopoulos Eggenschwiler, P., Arroyo Rojas Dasilva, Y., 2013. Metal particle emissions in the exhaust stream of diesel engines: an electron microscope study. Environ. Sci. Technol. 47, 14495–14501.

Ma, L., Li, M., Zhang, H.F., Li, L., Huang, Z.X., Gao, W., et al., 2016. Comparative analysis of chemical composition and sources of aerosol particles in urban Beijing during clear, hazy, and dusty days using single particle aerosol mass spectrometry. J. Clean. Prod. 112, 1319–1329.

McNeill, V.F., 2014. Atmospheric and Aerosol Chemistry. vol. 339. Springer Berlin Heidelberg, Berlin, Heidelberg.

Moffet, R.C., Prather, K.A., 2009. In-situ measurements of the mixing state and optical properties of soot with implications for radiative forcing estimates. Proc. Natl. Acad. Sci. U. S. A. 106, 11872–11877.

Moffet, R.C., de Foy, B., Molina, L.T., Molina, M.J., Prather, K.A., 2008. Measurement of ambient aerosols in northern Mexico City by single particle mass spectrometry. Atmos. Chem. Phys. 8, 4499–4516.

Odum, J.R., Jungkamp, T.P.W., Griffin, R.J., Flagan, R.C., Seinfeld, J.H., 1997. The atmospheric aerosol-forming potential of whole gasoline vapor. Science 276, 96–99.

Ortiz-Montalvo, D.L., Lim, Y.B., Perri, M.J., Seitzinger, S.P., Turpin, B.J., 2012. Volatility and yield of glycolaldehyde SOA formed through aqueous photochemistry and droplet evaporation. Aerosol Sci. Technol. 46, 1002–1014.

Pathak, R.K., Louie, P.K.K., Chan, C.K., 2004. Characteristics of aerosol acidity in Hong Kong. Atmos. Environ. 38, 2965–2974.

Pratt, K.A., Prather, K.A., 2009. Real-time, single-particle volatility, size, and chemical composition measurements of aged urban aerosols. Environ. Sci. Technol. 43, 8276–8282.

Pratt, K.A., Prather, K.A., 2012. Mass spectrometry of atmospheric aerosols–recent developments and applications. Part II: on-line mass spectrometry techniques. Mass Spectrom. Rev. 31, 17–48.

Pratt, K.A., Murphy, S.M., Subramanian, R., DeMott, P.J., Kok, G.L., Campos, T., et al., 2011. Flight-based chemical characterization of biomass burning aerosols within two prescribed burn smoke plumes. Atmos. Chem. Phys. 11, 12549–12565.

Qin, X., Pratt, K.A., Shields, L.G., Toner, S.M., Prather, K.A., 2012. Seasonal comparisons of single-particle chemical mixing state in Riverside, CA. Atmos. Environ. 59, 587–596.

Robinson, A.L., Donahue, N.M., Shrivastava, M.K., Weitkamp, E.A., Sage, A.M., Grieshop, A.P., et al., 2007. Rethinking organic aerosols: semivolatile emissions and photochemical aging. Science 315, 1259–1262.

Robinson, E.S., Saleh, R., Donahue, N.M., 2013. Organic aerosol mixing observed by single-particle mass spectrometry. J. Phys. Chem. A 117, 13935–13945.

Seinfeld, J.H., Pandis, S.N., 2012. Atmospheric Chemistry and Physics: From Air Pollution to Climate Change. John Wiley & Sons.

Seinfeld, J.H., Pandis, S.N., 2016. Atmospheric Chemistry and Physics: From Air Pollution to Climate Change. John Wiley & Sons.

Shen, Z., Cao, J., Liu, S., Zhu, C., Wang, X., Zhang, T., et al., 2011. Chemical composition of PM_{10} and $PM_{2.5}$ collected at ground level and 100 meters during a strong winter-time pollution episode in Xi'an, China. J. Air Waste Manage. Assoc. 61, 1150–1159.

Sodeman, D.A., Toner, S.M., Prather, K.A., 2005. Determination of single particle mass spectral signatures from light-duty vehicle emissions. Environ. Sci. Technol. 39, 4569–4580.

Song, X.-H., Hopke, P.K., Fergenson, D.P., Prather, K.A., 1999. Classification of single particles analyzed by ATOFMS using an artificial neural network, ART-2A. Anal. Chem. 71, 860–865.

Suess, D.T., Prather, K.A., 2002. Reproducibility of single particle chemical composition during a heavy duty diesel truck dynamometer study. Aerosol Sci. Technol. 36, 1139–1141.

Sun, Y.L., Wang, Z.F., Fu, P.Q., Yang, T., Jiang, Q., Dong, H.B., et al., 2013. Aerosol composition, sources and processes during wintertime in Beijing, China. Atmos. Chem. Phys. 13, 4577–4592.

Sun, J., Shen, Z., Cao, J., Zhang, L., Wu, T., Zhang, Q., et al., 2017. Particulate matters emitted from maize straw burning for winter heating in rural areas in Guanzhong Plain, China: current emission and future reduction. Atmos. Res. 184, 66–76.

Tao, J., Zhang, L., Cao, J., Zhang, R., 2017. A review of current knowledge concerning $PM_{2.5}$ chemical composition, aerosol optical properties and their relationships across China. Atmos. Chem. Phys. 17, 9485–9518.

Toner, S.M., Sodeman, D.A., Prather, K.A., 2006. Single particle characterization of ultrafine and accumulation mode particles from heavy duty diesel vehicles using aerosol time-of-flight mass spectrometry. Environ. Sci. Technol. 40, 3912–3921.

Toner, S.M., Shields, L.G., Sodeman, D.A., Prather, K.A., 2008. Using mass spectral source signatures to apportion exhaust particles from gasoline and diesel powered vehicles in a freeway study using UF-ATOFMS. Atmos. Environ. 42, 568–581.

Turšič, J., Berner, A., Podkrajšek, B., Grgić, I., 2004. Influence of ammonia on sulfate formation under haze conditions. Atmos. Environ. 38, 2789–2795.

Vaden, T.D., Song, C., Zaveri, R.A., Imre, D., Zelenyuk, A., 2010. Morphology of mixed primary and secondary organic particles and the adsorption of spectator organic gases during aerosol formation. Proc. Natl. Acad. Sci. 107, 6658–6663.

Wang, Y.C., Huang, R.J., Ni, H.Y., Chen, Y., Wang, Q.Y., Li, G.H., et al., 2017. Chemical composition, sources and secondary processes of aerosols in Baoji city of northwest China. Atmos. Environ. 158, 128–137.

Yang, F., Chen, H., Wang, X.N., Yang, X., Du, J.F., Chen, J.M., 2009. Single particle mass spectrometry of oxalic acid in ambient aerosols in Shanghai: mixing state and formation mechanism. Atmos. Environ. 43, 3876–3882.

Yao, X., Rehbein, P.J.G., Lee, C.J., Evans, G.J., Corbin, J., Jeong, C.-H., 2011. A study on the extent of neutralization of sulphate aerosol through laboratory and field experiments using an ATOFMS and a GPIC. Atmos. Environ. 45, 6251–6256.

Zhang, Y., Wang, X., Chen, H., Yang, X., Chen, J., Allen, J.O., 2009. Source apportionment of lead-containing aerosol particles in Shanghai using single particle mass spectrometry. Chemosphere 74, 501–507.

Zhang, G., Bi, X., Lou, S., Li, L., Wang, H., Wang, X., et al., 2014. Source and mixing state of iron-containing particles in Shanghai by individual particle analysis. Chemosphere 95, 9–16.

Zhang, R., Wang, G., Guo, S., Zamora, M.L., Ying, Q., Lin, Y., et al., 2015. Formation of urban fine particulate matter. Chem. Rev. 115, 3803–3855.

Zhou, Y., Xue, L., Wang, T., Gao, X., Wang, Z., Wang, X., et al., 2012. Characterization of aerosol acidity at a high mountain site in central eastern China. Atmos. Environ. 51, 11–20. https://doi.org/10.1016/j.atmosenv.2012.01.061.

Zuo, Y., Hoigné, J., 1994. Photochemical decomposition of oxalic, glyoxalic and pyruvic acid catalysed by iron in atmospheric waters. Atmos. Environ. 28, 1231–1239.